DUX4 regulates oocyte to embryo transition in human

Sanna Vuoristo[1,2#*], Christel Hydén-Granskog[3], Masahito Yoshihara[1], Lisa Gawriyski[4], Anastassius Damdimopoulos[5], Shruti Bhagat[1,6], Kosuke Hashimoto[6], Kaarel Krjutškov[1,7,8], Sini Ezer[8,9], Priit Paluoja[7], Karolina Lundin[2], Pauliina Paloviita[2], Gaëlle Recher[10], Vipin Ranga[11], Tomi Airenne[11], Mahlet Tamirat[11], Eeva-Mari Jouhilahti[8], Timo Otonkoski[8], Juha S. Tapanainen[2,3,12], Hideya Kawaji[6,13,14], Yasuhiro Murakawa[6,15], Thomas R. Bürglin[16], Markku Varjosalo[4], Mark S. Johnson[11], Timo Tuuri[2, 3], Shintaro Katayama[1,9*] and Juha Kere[1,8,9 *]

[1]Karolinska Institutet, Department of Biosciences and Nutrition, Huddinge, Sweden

[2]University of Helsinki, Department of Obstetrics and Gynecology, Helsinki, Finland

[3]Helsinki University Hospital, Department of Obstetrics and Gynecology, Helsinki, Finland

[4]University of Helsinki, Institute of Biotechnology, Helsinki, Finland

[5]Karolinska Institutet, Bioinformatics and Expression Analysis Core Facility, Huddinge, Sweden

[6]RIKEN Center for Integrative Medical Sciences, Yokohama, Japan

[7]Competence Centre for Health Technologies, Tartu, Estonia

[8] Stem Cells and Metabolism Research Program, University of Helsinki, Finland

[9]Folkhälsan Research Center, Helsinki, Finland

[10]Institut d'Optique Graduate School, CNRS - Université de Bordeaux, Talence, France

[11]Structural Bioinformatics Laboratory, Biochemistry, Faculty of Science and Engineering, Åbo Akademi University, Turku, Finland

[12]Oulu University Hospital, Oulu, Finland

[13]RIKEN Preventive Medicine and Diagnosis Innovation Program, Wako, Japan

[14]Tokyo Metropolitan Institute of Medical Science, Tokyo, Japan

[15]IFOM, The FIRC Institute of Molecular Oncology, Milan, Italy

[16]University of Basel, Department of Biomedicine, Basel, Switzerland

[#]Current affiliation

[*]Corresponding author

Abstract

In oocyte to embryo transition, the fertilized oocyte undergoes final maturation and the embryo genome is gradually activated during the first three cell divisions. How this transition is coordinated and which factors drive the processes in humans is largely unknown. Here we studied the role of the double homeodomain transcription factor DUX4 in regulating the human oocyte to embryo transition. DUX4 knockdown zygotes show delayed transcriptome reprogramming during the first three days after fertilization. Our combined experimental approaches allowed integrated analysis on the transcriptome, chromatin, and proteome data in human embryos or a DUX4 expressing human embryonic stem cell model. We conclude that DUX4 is a pioneering factor that regulates human oocyte to embryo transition through regulating oocyte mRNA degradation, as well as direct binding and activation of minor genome activation genes, and genomic repeat elements.

Mammalian pre-implantation development involves a series of coordinated processes, starting with oocyte to embryo transition (OET). OET is a major developmental reprogramming event from the oocyte to a totipotent embryo, involving fundamental changes in the epigenetic landscapes, degradation of maternal mRNAs, and embryonic genome activation (EGA)[1]. In humans, the major EGA takes place by the 8-cell stage[2-4]. Minor EGA genes are upregulated in the human 4-cell embryos where they subsequently induce genes upregulated at the major EGA[3]. Until now, most studies focusing on human EGA have concentrated on the genes that are expressed in the cleavage stage (2-cell, 4-cell, and 8-cell) embryos[3,5] and set the stage for the forthcoming lineage commitment[6,7]. How OET and EGA are orchestrated in the human embryos and which genes act as pioneers remain poorly understood.

The conserved double homeodomain transcription factor DUX4 is expressed in early human embryos[8-10]. It represents a plausible candidate to regulate the OET in humans, given its capacity to activate EGA-related genes and the genomic repeat elements[8,9]. In this work we have used a combination of methods to investigate DUX4 in the course of early human development. Our data highlight DUX4 mRNA upregulation already in the zygotes followed by down-regulation within the next cell division. Abundant cytoplasmic and nuclear DUX4 protein was apparent only during the first two days of development. Our in-depth characterisation of DUX4 in the human embryos suggested that it is not required for survival of the human embryos during the first three days of development but that DUX4 regulates OET in the human. siRNA silencing of DUX4 in zygotes delayed oocyte mRNA degradation. Our comprehensive analysis of transcriptome and chromatin data in human embryos or DUX4 expressing cell lines suggested that DUX4 opens up chromatin through direct

activation of the retroelements and unannotated genomic regions. Our protein interaction data demonstrated that DUX4 interacts with transcriptional mediators, chromatin modifiers, and ubiquitinases expressed in the human oocytes and early embryos. We conclude that DUX4 regulates different aspects of the OET in humans by affecting mRNA degradation, transcriptional regulation and chromatin structure.

Results

DUX4 is transiently expressed immediately after fertilization

We first measured DUX4 mRNA levels in human MII oocytes (N=20), zygotes (N=59), and cleavage embryos (2-cell, N=4; 4-cell, N=14; 8-cell, N=15). We found significant DUX4 upregulation in the zygotes, while few transcripts were found in the MII oocytes or the cleavage embryos[10-13] (Fig. 1a). The expression of the DUX is evolutionary conserved as shown by stage-specific expression in mouse, bovine, and non-human primates[14]. We stained embryos with a monoclonal antibody targeting the DUX4 protein and detected cytoplasmic DUX4 in the zygotes and all cleavage embryos although less in 8-cell embryos (Fig. 1b). DUX4 protein was abundantly present in the nuclei of the 2- and 4-cell embryos whereas nuclei of the 8-cell embryos were mostly negative (Fig. 1b). In a single early 8-cell stage embryo there was high variability in the nuclear DUX4 staining, consistent with a snapshot of on-going degradation. We quantified nuclear DUX4 intensities in 3D and normalized them to the cytoplasmic DUX4 intensities and found variable but increasing nuclear signal from the zygotes up to the 4-cell embryos, while nuclear DUX4 was low or absent in the 8-cell embryos (Fig 1c). These results demonstrated that DUX4 transcription takes place immediately after fertilisation and is followed by cytoplasmic and nuclear localisation of the DUX4 protein during the first two days of human embryo development.

DUX4 protein may form a relatively stable structure even when not bound to DNA

Given predominant DUX4 protein presence in the cytoplasm of the embryos as well as stage-specific nuclear localization, we analysed the structural features of DUX4

(Fig. 2). Human DUX4 comprises two homeodomains (HD1: residues 19-81; and HD2: 94-153; UniProt numbering), an intrinsically disordered region (IDR: 154-370) and a C-terminal domain (residues 371-424; Fig. 2a). A stretch of hydrophobic residues (308-323) within IDR is conserved in primates and could have a regulatory role by interacting with other transcription co-regulators or masking the C-terminal domain from solvent when no interacting partners are present. The C-terminal domain is predicted to have two structurally ordered and evolutionarily conserved regions: residues 371-387 and residues 414-423 (Fig. 2a). As a secondary structure the C-terminal domain is predicted to contain three alpha helices and may form a stable fold similar to that revealed by NMR for the Pax8 paired box domain (PDB: 2K27;[15]). We found a nine amino acid transactivation domain (9aaTAD) located at the C-terminal domain (371-379), also recently reported by Mitsuhashi et al.[16]. This motif is also present in the PRD-like homeoprotein LEUTX[17] and might be recognized by other proteins involved in the regulation of transcription, similar to the 9aaTAD motif of the MLL that interacts with the cAMP-response element binding protein, a transcriptional co-activator[18].

In the crystal structure of DUX4 (PDB: 6E8C;[19]) HD1 and HD2 bind DNA in a symmetric manner (Fig. 2b). Residue R21, located at the N-terminal loop of HD1, interacts with the residues I121, E135 and Q139 of HD2 and, equivalently, R96 located at the N-terminal arm of the HD2 interacts with the residues I46, E60 and Q64 of HD1 (Fig. 2b, c, d). Moreover, the main-chain carbonyl groups of G19 of HD1 and G94 of HD2 respectively form a hydrogen bond with the main-chain nitrogen atom of I121 of HD2 and I46 of HD1. We next asked whether these residues are conserved within the DUX family of homeoproteins and within primates (Fig. 2e): based on our

151 sequence alignment, residues equivalent to G19, R21, I46, E60, Q64, G94, R96, I121,
152 E135 and Q139 of DUX4 are highly conserved. Interestingly, the residues G19, R21,
153 I46, E60, Q64, G94, R96, I121, E135 and Q139 of DUX4 (Fig. 2c,d) are not directly
154 involved in DNA binding, which prompted us to speculate that these residues could
155 be important for locking HD1 and HD2 together as a unit before DNA binding, a
156 hypothesis, which we further tested using molecular dynamics (MD) simulations.

157

158 Based on MD simulations and the RMSD among snapshots made every 10 ps (Fig.
159 2f), the DUX4 HD2-DNA complex appeared the most stable complex (average
160 RMSD over backbone atoms of 1.73 Å), followed by DUX4-DNA (1.77 Å) and
161 DUX4 HD1-DNA complex (2.3 Å). The DNA-free DUX4 HD1-HD2 structure (4.0
162 Å) was the least stabile yet the interactions between HD1 and HD2 were maintained
163 over the 100 ns simulation. Indeed, ionic interactions between R96 of HD2 and E50
164 and E60 of HD1 seem to be fundamental for the stability of the double HD structure
165 of DUX4: the electrostatic interactions/hydrogen bonds between R96 and E60 were
166 present during 92% of the simulation time. Additional stabilizing interactions between
167 the two HDs also take place between R21 (HD1) and E135 (HD2), and R22 (HD1)
168 and E125 (HD2). While these charged interactions hold the two HDs together, the
169 intermediate linker loop imparts flexibility, which could be vital to accommodate
170 DNA once DUX4 enters the nucleus and locates its binding motif. Even with bound
171 DNA, the linker loop fluctuates more relative to HD1 and HD2, as observed from the
172 RMSF values for the CA atoms of residues of the DUX4-DNA structure (Fig. 2g).

173

DUX4 protein interacts with transcriptional mediators and chromatin modifiers

Abundant nuclear and cytoplasmic DUX4 in the human embryos and the modelled stable structure of the DUX4 when not bound to DNA suggested that DUX4 might have functions beyond DNA binding. To study this, we applied a recently published MAC-tag method to identify DUX4 protein-to-protein interactions[20,21]. We identified altogether 158 BioID and 43 AP-MS high-confidence DUX4 interactions, out of which 19 appeared in both datasets (FDR < 0.05, corresponding to > 0.73 SAINT Score). Single BioID interactions and AP-MS interactions together with the interactions that appeared in both data sets, based on the scored frequency of interaction with DUX4, are shown in Fig 3a. We concentrated on the DUX4 interacting proteins that scored above the median value (Fig 3b). Overrepresentation Enrichment Analysis (ORA) of protein pathway markers (Reactome, KEGG) showed significant enrichment ($p < 0.05$, FDR < 0.01) of markers linked to generic transcription and 'RNA Polymerase II Transcription', 'Chromatin organization' and 'Chromatin modifying enzymes'. Comparing our list of genes to protein complex databases such as ComplexPortal and Corum using Fisher's Exact Test yielded significant overrepresentation of several variants of the SWI/SNF ATP-dependent chromatin remodelling complex, Core mediator complex, NSL histone acetyltransferase complex, SRCAP histone exchanging complex and the NuA4 histone acetyltransferase complex ($p < 0.05$, FDR 0.01) (Fig. 3b). There were 28 DUX4 interacting proteins classified as RNA binding (GO:0003723) and 19 out of these were linked to spliceosome and pre-mRNA-splicing. In the protein complex database Corum, DUX4 interactors were significantly overrepresented in the Spliceosome, with 10 interactors comprising 7% of the whole complex. In addition, we found six DUX4 interacting proteins (ZSCAN4, ZSCAN5C, ZSCAN5D, RFPLA,

199 RFPLB, RNF8, PTOV1, and MB3LB) that have not appeared in the analyses of other
200 transcription factors. As the protein interaction assay was run in a non-embryonic cell
201 line (HEK), we next studied which of the identified DUX4 interacting proteins are
202 expressed by human oocytes or embryos[3,11]. Importantly, the vast majority of the
203 genes coding for the DUX4 interacting proteins were expressed in oocytes (maternal
204 genes), embryos, or both. These results suggested that DUX4 could potentially
205 regulate maternal and embryonic proteins in the cytoplasm and nucleus during the
206 OET.

207

208 *Knock-down of DUX4 in human zygotes leads to dysregulation of the maternal*
209 *transcriptome*

210 We next asked how DUX4 regulates the OET and early human embryo development.
211 We microinjected either DUX4 targeting siRNA (siDUX4) or control siRNA
212 (siCTRL) together with GAP-GFP mRNA to triploid human zygotes and followed
213 their development for 48 h after the microinjections, until the third day of
214 development (Fig 4a). 18 h after microinjection, GAP-GFP protein was expressed in
215 all embryos, confirming successful microinjections. Staining for the DUX4 protein
216 was very faint or absent in the siDUX4 embryos but strongly positive in the siCTRL
217 embryos 24 h after microinjection, showing that the DUX4 targeting siRNA
218 efficiently down-regulated DUX4 (Fig 4b). The cells from the embryos were
219 collected 48 h after microinjections for single-cell-tagged reverse transcription RNA
220 sequencing (STRT RNA-seq[22,23]), which detects the transcript far 5'-ends (TFEs).
221 siDUX4 embryos did not arrest during the experiment by live imaging follow-up, but
222 their transcriptome was dysregulated in comparison to that of the siCTRL embryos. A

number of transcripts downregulated in the siCTRL appeared enriched in the siDUX4 embryos (Fig. 4c). In order to study how the siDUX4 enriched transcripts typically behave during the first three days of development, we next compared siDUX4 and siCTRL embryos to our published gene expression data set[3,10] on human MII oocytes, zygotes, and cleavage cells. These analyses further confirmed that a large number of TFEs that remained enriched in the siDUX4 embryos were typically downregulated between the oocytes and the 4-cell embryos (Fig 4d), the zygotes and the 4-cell embryos (Fig 4e), and the 4-cell and 8-cell embryos (Fig 4f), indicating delayed degradation of the maternal transcripts. Gene expression enrichment analysis using TopAnat[24] for the altogether 91 genes enriched in siDUX4 embryos resulted in terms such as 'female germ cell' and 'oocyte', in agreement with non-degraded maternal transcripts. As shown for the siDUX4 enriched gene set, a number of well-known maternal genes such as *GDF9*, *ZP1*, *ZP2*, *ZP3*, *KHDC3L*, *WEE2*, *NPM3*, *TUBB8*, and *RERE* failed to downregulate (Fig. 4g), demonstrating that the OET remained incomplete after DUX4 abolishment in human zygotes.

DUX4 directly activates the minor EGA genes and a number of unannotated regions

We next generated two TetOn-DUX4 human embryonic stem cell (hESC) lines expressing DUX4-ires-EmGFP under doxycycline, and studied the effects of DUX4 on the activity and accessibility of the genome (Fig 5a). *DUX4* mRNA (Fig 5b) and protein (Fig 5c) expression promptly followed doxycycline induction and the known DUX4 target genes *ZSCAN4* and *TRIM48* followed the induction with slight delay (Fig 5b). We performed bulk RNA-seq using STRT RNA-seq methods and the data analysis of the sorted EmGFP+ DUX4 expressing cells showed roughly equal

numbers of up- and downregulated TFEs (Fig 5d). Notably, the majority of the upregulated TFEs were mapped to unannotated genomic regions, whereas the downregulated TFEs were mapped to protein coding regions (Fig 5d). The known target genes of DUX4, i.e., *ZSCAN4*, *LEUTX* and *TRIM48* were significantly upregulated in the EmGFP+ cells (Fig 5e). Downregulated protein-coding TFEs included a number of ribosomal genes and genes maintaining pluripotency. This is in agreement with previous findings showing that DUX4 downregulates some pluripotency markers[25]. We integrated the data from our RNA-seq and published DUX4 ChIP-seq analysis[26,27] and found that out of the 32 minor EGA genes induced in 4-cell embryos[3], 23 were induced in the EmGFP+ cells and 17 out of these overlapped with DUX4 binding sites. This suggested that DUX4 can induce the majority of the minor EGA-related genes (Fig 5f). We also identified three previously unannotated DUX4 targets *KHDC1* pseudogene 1 (FE463525; Fig 5e and 6a), RING-finger type E3 ubiquitin ligase (FE533694; Fig 5e and 6b), and RING-finger domain protein 4.2 (FE130507; Fig 5e and 6c) that were induced in 4-cell embryos[3], were upregulated by DUX4, and overlapped with DUX4 binding sites. We cloned novel DUX4 target transcripts from a cDNA pool of human day 4 embryos, confirming their presence in early human cleavage embryos (Fig 6). On the other hand, out of the 129 major EGA genes upregulated in 8-cell human embryos[3], 14 were upregulated by DUX4 and interestingly, 33 were downregulated (Fig 5f). These data suggested that DUX4 could upregulate some major EGA genes, but that most of them are likely activated by the minor EGA genes (such as LEUTX[28]), and that DUX4 might also negatively regulate major EGA genes. DUX4-induced TFEs were highly enriched with DUX4 binding sites[26,27] (Fig 5g), and the most highly enriched motif in the DUX4-induced TFEs was similar to the known DUX4 motif[29] (Fig 5h). Furthermore,

these TFEs were remarkably overrepresented with the DUX4 binding sites among hundreds of transcription factors (Fig 5i).

Ectopic DUX4 expression causes chromatin opening at ERVL-MaLR elements similar to 2-cell human embryos

We next integrated STRT RNA-seq and ATAC-seq data from EmGFP +/- sorted TetOn-Dux4 hESC. DUX4 expression lead to consistent modifications in chromatin accessibility across all studied clones (Fig 7a). The transcriptionally upregulated TFEs correlated with more accessible (gained) genomic regions in the DUX4 induced cells while the correlation was less obvious for the downregulated TFEs and less accessible (lost) chromatin (Fig 7a). We found that the gained chromatin regions correlated with upregulated TFEs and lost chromatin regions correlated with downregulated TFEs (Fig 7b), likely implying that the transcriptional downregulation induced by DUX4 expression is faster than the nucleosome-mediated closing of the chromatin (Fig 7a and b). We then asked how DUX4 expression modified openness of the different regions of the chromatin. In general, DUX4 rapidly caused chromatin remodelling, especially chromatin opening, far from transcription start sites (TSS), demonstrating that the TSSs seem to be less targeted by the DUX4 expression than other genomic regions (Fig 7c). We next focused on the ATAC-gained chromatin sites. These chromatin regions were remarkably enriched with DUX4 binding sites compared with unchanged regions ($P<2.2e-16$). Out of the ATAC-gained chromatin sites, 48.9% overlapped with ERVL-MaLR elements and they were significantly enriched for the DUX4 binding sites compared with non ERVL-MaLR overlapping sites (55.8% $P < 2.2e-16$) (Fig. 7d). The ATAC-gained ERVL-MaLR regions remarkably overlapped

296 with the open chromatin regions found in 2-cell human embryos[30] (Fig. 7e). Out of
297 the DUX4 induced gained chromatin regions that overlapped with those of the 2-cell
298 embryos, upregulated by DUX4 induction, and overlapped with DUX4 binding sites,
299 76.7% were unannotated. Only few protein-coding genes, for instance *ZSCAN4* and
300 the transcriptional and chromatin regulators *KDM5B (JARID1B)* and *ZNF296* were
301 included. These results show that DUX4 directly binds ERVL-MaLR elements and
302 converts the chromatin landscape of the hESCs towards that of the human 2-cell
303 embryos. These data also suggest that DUX4 largely functions through yet
304 unannotated genomic regions.

305

Discussion

The OET, including fertilization and activation of the oocyte to totipotent blastomeres and subsequent EGA, gradually sets the stage for embryo development[31-33]. How the OET is orchestrated in human and which factors are the main drivers are still poorly known. One of the potential candidates driving the OET in human embryos is DUX4. Our data here show that DUX4 transcripts appear immediately after fertilisation and are downregulated rapidly following the first and the second cleavage divisions. The origin of *DUX4* transcripts is still unclear. It could be one of the maternal dormant RNAs, supported by the fact that DUX4 was absent in the majority of the oocytes but was significantly induced in the zygotes. Dormant maternal RNAs are stored in the oocytes as deadenylated transcripts and they are polyadenylated and translated only after resumption of meiosis or after fertilisation[34]. The increasing nuclear DUX4 protein intensity from zygotes to 4-cell embryos and its disappearance in the nuclei of 8-cell embryos suggested that DUX4 can modify transcriptome and chromatin of the embryos already before the genome activation takes place. Detailed mechanisms of DUX4 protein degradation in the 8-cell embryos remain to be further investigated; however, DUX4 upregulated and interacted with several protein ubiquitinases, such as TRIM48, a well-known DUX4 target gene. We also identified two previously unannotated and possibly embryo-specific putative RING-finger type E3 ubiquitin ligases that were expressed in early human embryos and induced by DUX4. The putative ubiquitinases RFPLA (RFPL4A) and RFPLB (RFPL4B) regulate protein degradation in germ cells[35,36]. Another ubiquitin-ligase, RNF114, was recently shown to be essential for the OET in the mouse[37]. Taken together, our data suggested that DUX4 induces expression of ubiquitin ligases and also interacts with ubiquitinases,

possibly regulating the presence of DUX4 itself as well as general proteome during OET.

Knock-down of DUX4 in the human zygotes did not cause mitotic arrest during the 2-day experiment, in agreement with recent findings on Dux in mouse embryos where a minority of embryos may proceed until blastocyst stage[8,38,39]. In the mouse Dux-/- embryos, around 30% of the EGA transcripts that should be upregulated were downregulated[39], while in the human DUX4 knock-down embryos, many of the maternal, normally downregulated genes remained unchanged, suggesting that Dux/DUX4 alone is sufficient for neither the OET nor the EGA. Another candidate gene regulating OET is *PLAG1*[40]. De novo PLAG1 binding site is found in the EGA genes in the human embryos, and the phenotype of Plag1+/- mice lacking the maternal *Plag1* allele show enriched expression of maternal transcripts at the 2-cell stage, when major EGA occurs in the mouse. The question remains how DUX4, together with other factors such as PLAG1, coordinates regulation of the maternal and EGA transcripts in human and which yet unnamed genes might be involved in the OET in human.

Ectopic expression of DUX4 in the hESC caused opening of the chromatin regions outside of TSSs, largely at ERVL-MaLR elements. Dux binding at *Mervl* loci drives chromatin reorganisation at *Mervl* loci in the mouse 2-cell embryo-like cells, and chromatin organisation during early mouse development is a consequence of the *Mervl* integration[41]. Human 2-cell-like cells have not been established by now, but importantly, in our experiments binding of the DUX4 at ERVL-MaLR elements[14]

could modify chromatin towards embryo-like stage even in the hESCs. Long terminal repeat elements abundantly present in the genome have been suggested as key elements contributing to the OET, when major epigenetic and chromatin changes take place[42]. Our integrated analysis on chromatin openness and transcriptional regulation, together with the DUX4 ChIP-seq data[26,27] demonstrated that DUX4 regulates several transcripts and the corresponding genomic loci coding for chromatin modifiers and epigenetic regulators, as also suggested by Liu et al.[43]. Taken together, our data indicate that DUX4 alone is not a sufficient inducer for the first three days of human embryo development but that it regulates the OET by regulating maternal RNA degradation, EGA genes, and repetitive elements, all of which have been shown to be crucial for the successful OET in organisms other than human. In addition to regulating genetic elements by DNA-binding, DUX4 may regulate the proteome by inducing ubiquitination pathway genes during the OET in human.

Online methods

Human pre-implantation embryos for single cell RNA-sequencing using STRT method

We analysed single cell RNA-sequencing data from Töhönen et al.[3] for MII oocytes (N=20), zygotes (N=59), 2-cell (N=4), 4-cell (N=15) and 8-cell (N=14) embryos. For the DUX4 knockdown experiment 18 siCTRL cells (N=2) and 18 siDUX4 cells (N=3) were analysed. The embryos were incubated in Ca^{2+}/Mg^{2+} -free culture medium (Biopsy Medium, Origio) at 37°C heated stage for separation of the cells. Individuals cells were briefly rinsed in Ca^{2+}/Mg^{2+} -free PBS and placed directly in lysis buffer (5mM Tris-HCl, pH 7.0 (LifeTechnologies); 5mM DTT (Thermo Scientific), 0.02 % Tx100 (Fisher Scientific); 0.5 U/µl Ribolock RNAse inhibitor (ThermoFisher)). The library was prepared according to the published protocol[3,22,44]. The amplified libraries were sequenced on the Illumina HiSeq 2000 instrument.

Bulk RNA-sequencing using STRT method

Total RNA was isolated from the FAC-sorted DUX4-TetOn hESCs using the RNAqueous Total RNA Isolation Kit (AM1912; ThermoFisherScientific). 20ng of total RNA from each sample was used for library preparations. The libraries were prepared using the STRT method as above, with minor modifications. Briefly, RNA samples were placed in a 48-well plate in which a universal primer, template-switching oligos, and a well-specific 8-bp barcode sequence (for sample identification) were added to each well[23,45]. The synthesized cDNAs from the samples were then pooled into one library and amplified by single-primer PCR with the

395 universal primer sequence. The resulting amplified library was then sequenced using
396 the Illumina NextSeq 500 instrument.

397

398 *Preprocess of raw STRT RNAseq reads*

399 The sequenced STRT raw reads were processed by STRTprep[23], v3dev branch
400 91a62d2 commit at https://github.com/shka/STRTprep/tree/v3dev. The processed
401 nonredundant reads were aligned to hg19 human reference genome sequences, ERCC
402 spike-in sequences and human ribosomal DNA unit (GenBank: U13369) with RefSeq
403 transcript alignments as a guide of exon junctions. For gene-based statistics, uniquely
404 mapped reads within (i) the 5'-UTR or the proximal upstream (up to 500 bp) of the
405 RefSeq protein coding genes, and (ii) within the first 50 bp of spike-in sequences,
406 were counted. For TFE-based statistics, the mapped reads were assembled according
407 to the alignments, and uniquely mapped reads within the first exons of the assembled
408 transcripts were counted, as described in Töhönen et al 2015[3].

409

410 *Downstream STRT RNA-sequencing data analysis*

411 Differentially expressed genes and TFEs required significantly different tendency on
412 the expression levels between two groups (q-value < 0.05), and significantly larger
413 variation than the technical variation (adjusted p-value < 0.05 by BH correction). The
414 former tendency was tested by the R package SAMstrt v0.99.0[45], and the latter
415 variation (fluctuation) was estimated based on gene-to-spikein (or TFE-to-spikein)
416 ratios in the squared coefficient of variation, described in Supplementary Text 1 of
417 Krjutskov et al. 2016[23]. The minimum value but non-zero was added to all the

418 normalized read counts and then the counts were divided by the minimum value so
419 that the logarithm of zero counts become zero. Enrichment analysis of anatomical
420 terms for the list of upregulated genes by siDUX4 was performed using the TopAnat[24]
421 (https://bgee.org/?page=top_anat). All human genes in the Bgee database were used
422 as background. STRT data of human early embryo were obtained from Töhönen et al.
423 2015 and 2017[3,10] and were overlapped with TFEs using the intersectBed function
424 from BEDTools[46] (v2.27.1). DUX4 ChIP-seq data was obtained from GSE33838[26]
425 and scores around the FEs were calculated with computeMatrix and visualized with
426 plotProfile from deepTools[47] (v3.1.3). Motif enrichment was analyzed using the
427 command findMotifsGenome.pl from HOMER[48] (v4.10.3) with the option "-size -
428 300,100". Enrichment analysis with publicly available ChIP-seq datasets was
429 conducted with ChIP-Atlas[49] (http://chip-atlas.org). A total of 7,216 human
430 transcription factor ChIP-seq datasets which had more than 500 peaks were analyzed.
431 Fold enrichment was calculated as (the number of ChIP-seq peaks overlapping with
432 upregulated TFEs / the number of upregulated TFEs) / (the number of ChIP-seq peaks
433 overlapping with all TFEs / the number of all TFEs). *P*-values were calculated with
434 Fisher's exact test and *Q*-values were calculated with the Benjamini & Hochberg
435 method. After excluding the TFEs annotated on ribosomal DNA, 6,425 upregulated
436 TFEs were used as foreground and 109,624 all the detected TFEs were used as
437 background both in the motif and ChIP-seq enrichment analysis.

438

439 *Human ESC culture*

440 hESC lines H1 (WA01) and H9 (WA09) were purchased from WiCell. The hESCs
441 were maintained on Geltrex-coated tissue culture dishes in Essential 8 culture medium

and passaged every three to five days by incubation with 0.5 mM EDTA (all from Thermo Fisher Scientific).

Plasmid construction

The full-length DUX4 (NM_001293798.2) was synthesized and cloned between the SalI and BamHI sites of the pB-tight-hMAFA-ires-EmGFP-pA-PGK-Puro vector (a kind gift from Diego Balboa, Biomedicum Stem Cell Centre) at GenScript (Genscript, NJ, USA).

Doxycycline-inducible DUX4 expressing human ESCs

The hESCs were incubated with StemPro Accutase (Thermo Fisher Scientific) until the edges of the colonies started to curl up. The Accutase was aspirated and the cells were gently detached in cold 5% FBS (Thermo Fisher Scientific) -PBS (Corning) and counted. One million cells were centrifuged at 800rpm for 5 min and the pellet was transferred into 120 µl of R-buffer containing 1 µg of pB-tight-DUX4-ires-EmGFP-pA-PGK-Puro, 0.5 µg of pBASE and 0.5 µg of rtTA-M2-IN plasmids. 100 µl of the cell-plasmid suspension was electroporated with two pulses of 1100 V, 20 ms pulse width, using Neon Transfection system. The electroporated cells were plated on Geltrex-coated dishes in Essential 8 medium with 10 µM ROCK inhibitor Y27632 (Peprotech). Fresh Essential 8 medium without ROCK-inhibitor was changed to the cells on the day following the electroporation. The cells were selected with Puromycin at 0.3 µg/mL. The TetOn-DUX4 hESC clones were picked manually on Geltrex-coated 96-well plates, expanded and selected again with Puromycin.

Appearance of the EmGFP reporter protein was tested using Doxycycline at concentrations ranging from 0.2 μg/ml to 1.0 μg/ml and detected using EVOS FL Cell imaging system (Thermo Fisher Scientific). When indicated for the experiments presented in this paper, the EmGFP+ DUX4 expressing hESC clones had been treated with 1μg/ml of Doxicycline for 1, 2, 3, (qPCR) or 4 hours prior to downstream analyses.

cDNA cloning of unannotated DUX4 targets

Single human 4-cell embryo cDNA library was prepared according to the protocol by Tang et al.[50] and used for cloning of the putative transcripts. The transcripts were amplified using Phusion High-Fidelity DNA polymerase (New England Biolabs) according to manufacturer's instructions. Predicted KHDC1 pseudo gene 1, putative RING-finger type E3 ubiquitin ligase and putative RING-finger domain protein encoding genes were amplified using touchdown PCR: 98˚C for 30 s; 24 cycles of 98˚C for 10 s, annealing for 30 s, temperature decreasing from 63˚C to 56˚C, 1 ˚C/3 cycles, 72˚C for 30 s; 16 cycles of 98 ˚C for 10 s, 55˚C for 30 s, 72˚C for 30 s; final extension 72˚C for 10 min. All PCR products were cloned into pCR4Blunt-TOPO vector using Zero Blunt TOPO PCR Cloning kit (Invitrogen) and sequences were verified by Sanger sequencing (Eurofins Genomics). Clone sequences are available from the ENA browser at http://www.ebi.ac.uk/ena/data/view/LR694082-LR694089.

Bioinformatics analysis and molecular dynamics simulations of the DUX4 protein

The sequence for the human DUX4 (Q9UBX2) protein was obtained from the UniProt database (The UniProt Consortium[30]), whereas other sequences were

retrieved from the non-redundant database of NCBI using blastp[51] and with human DUX4 as the query sequence. Multiple sequence alignment was carried out using MAFFT[52]. Secondary structures, solvent accessibility and disordered regions were predicted using POLYVIEW-2D[53], SABLE[54], SCRATCH[55] and RaptorX-Property[56]. The 9aaTAD web server[57] was used to predict 9aaTAD motifs. The 2.12 Å resolution crystal structure of the DUX4 HD1-linker-HD2 fragment bound to DNA[19] (PDB: 6E8C) was obtained from the Protein Data Bank[58]. PyMOL (version 1.6; Schrödinger LLC) and Bodil[59] were used to analyze inter-HD interactions. Based on the DUX4 structure, molecular dynamics (MD) simulations, over all atoms, were used to explore the dynamic states of the (1) double HD complex with (HD1-HD2 + DNA) and (2) without (HD1-HD2) bound DNA and the individual HDs with bound DNA: (3) HD1 + DNA and (4) HD2 + DNA. MD simulations of these four structures were carried out with the AMBER package[60] (version 18) using the ff14SB[61] (for protein) and OL15[62] (for DNA) force fields. The structures were solvated with explicit TIP3P water molecules[63] within an octahedral box ensuring a 12 Å distance between the boundaries of the simulation box and solute atoms. Sodium counter ions were added to neutralize the system and additional Na^+/Cl^- ions were added to bring the salt concentration to 150 mM. Periodic boundary conditions were employed and the particle-mesh Ewald algorithm[64] was applied to electrostatic interactions with a distance cutoff of 9 Å.

Prior to the production simulation, 5000 cycles of steepest descent and conjugate gradient energy minimization were carried out on each system, initiated by introducing a 25 kcal mol^{-1} $Å^{-2}$ restraint on solute atoms that was gradually reduced to 0 kcal mol^{-1} $Å^{-2}$ over the total minimization. The systems were then heated from

514 100 K to 300 K during 100 ps with a 10 kcal mol^{-1} $Å^{-2}$ restraint on solute atoms,
515 followed by a 900 ps equilibration at constant pressure while systematically reducing
516 the restraint to 0.1 kcal mol^{-1} $Å^{-2}$. The equilibration protocol was finalized with a
517 restraint-free 5 ns simulation. The production simulation was performed for 100 ns at
518 constant temperature (300 K) and pressure (1 bar), which was maintained using the
519 Berendsen algorithm[65] with 5 ps coupling constant. Trajectories were saved every 10
520 ps and the resulting structural snapshots were analyzed further by calculating the root-
521 mean-square deviations (RMSD; over backbone atoms) and root-mean-square
522 fluctuations (RMSF; over C α atoms), as well monitoring hydrogen bond interactions
523 using the programs CPPTRAJ[66] and VMD[67].

524

525 *Affinity purification of protein complexes, mass spectrometry and data analysis*

526 *Cell Culture and Affinity Purification*

527

528 *Cloning of DUX4 to MAC-tag Gateway® destination vector*

529 DUX4 was first amplified in two-step PCR reaction from pB-tight-DUX4-ires-
530 EmGFP-pA-PGK-Puro and cloned to Gateway compatible entry clone using Gateway
531 BP Clonase II (Invitrogen) according to manufacturer's instructions. The entry clone
532 was further cloned to Gateway compatible destination vectors containing the C-
533 terminal and N-terminal tags as described[21]. Transfection and selection of the T-Rex
534 293 cells (Invitrogen, Life Technologies, R78007, cultured in manufacturer's
535 recommended conditions) and affinity purification of the final product was done as
536 previously[21].

537

538 *Liquid Chromatography-Mass Spectrometry*

539 Analysis was performed on a Q-Exactive mass spectrometer with an EASY-nLC 1000
540 system via an electrospray ionization sprayer (Thermo Fisher Scientific), using
541 Xcalibur version 3.0.63. Peptides were eluted from the sample with a C18 precolumn
542 (Acclaim PepMap 100, 75 µm x 2 cm, 3 µm, 100 Å; Thermo Scientific) and
543 analytical column (Acclaim PepMap RSLC, 65 µm x 15 cm, 2 µm, 100 Å; Thermo
544 Scientific), using a 60 minute buffer gradient ranging from 5 to 35% Buffer B, then a
545 5 min gradient from 35 to 80% Buffer B and 10 minute gradient from 80 to 100%
546 Buffer B (0.1% formic acid in 98% acetonitrile and 2% HPLC grade water). 4 µl of
547 peptide sample was loaded by a cooled autosampler. Data-dependent FTMS
548 acquisition was in positive ion mode for 80 min. A full scan (200-2000 m/z) was
549 performed with a resolution of 70,000 followed by top10 CID-MS^2 ion trap scans with
550 a resolution of 17,500. Dynamic exclusion was set for 30 s. Database search was
551 performed with Proteome Discoverer 1.4 (Thermo Scientific) using the SEQUEST
552 search engine on the Reviewed human proteome in UniProtKB/SwissProt databases
553 (http://www.uniprot.org, downloaded Nov. 2018). Trypsin was selected as the
554 cleavage enzyme and maximum of 2 missed cleavages were permitted, precursor
555 mass tolerance at ±15 ppm and fragment mass tolerance at 0.05 Da.
556 Carbamidomethylation of cysteine was defined as a static modification. Oxidation of
557 methionine and biotinylation of lysine and N-termini were set as variable
558 modifications. All reported data were based on high-confidence peptides assigned in
559 Proteome Discoverer (FDR < 0.01).

560

Identification of statistical confidence of interactions

Significance Analysis of INTeractome (SAINT[68]) -express version 3.6.3 and Contaminant Repository for Affinity Purification (CRAPome, http://www.crapome.org) were used to discover statistically significant interactions from the AP-MS data[69]. The DUX4 LC-MS data was ran alongside a large dataset of other transcription factors, as well as a large GFP control set. Final results represent proteins with a SAINT score higher than 0.73, and present in all four replicates.

Overrepresentation Analysis

Overrepresentation analysis of statistically significant interactions in Gene Ontology and Reactome was done in WebGestalt[70], and overrepresentation of prey proteins in ComplexPortal[71] (https://www.ebi.ac.uk/complexportal) and CORUM[72] (https://mips.helmholtz-muenchen.de/corum/) was done using Fisher's exact test and multiple testing correction in an in-house R-script.

Interaction network

Protein interaction networks were constructed from filtered SAINT data that was imported to Cytoscape 3.6.0. Known prey-prey interactions were obtained from the iRef database (http://irefindex.org).

RNA isolation, reverse transcription and quantitative real-time quantitative PCR

Total RNA was isolated by NucleoSpin RNA kit (Macherey Nagel). 1µg of RNA was reverse transcribed by MMLV-RTase with oligodT, dNTPs, and Ribolock in MMLV-RTase buffer (Thermo Fisher Scientific). 5X HOT FirelPol qPCR Mix (Solis Biodyne) was used to measure relative mRNA levels with Lightcycler (Roche). Δ Δ CT method was followed to quantify relative gene expression where *CYCLOPHILIN G* was used as endogenous control. Relative expression of each gene was normalized to the expression without doxycycline treatment.

Fluorescence associated cell sorting

TetOn-DUX4 hESCs were treated with TrypLE for 5 min and suspended into cold FACS buffer (5% FBS-PBS). Single cell suspension was filtered through 40µm Cell strainers and centrifuged at 800 rpm for 5min. The cell pellets were suspended in cold FACS buffer and placed on ice. EmGFP- and EmGFP+ cells were separated to FACS buffer by Sony SH800Z Cell Sorter with blue laser (488) and 100 µm nozzle.

ATAC-sequencing library preparation and data analysis

In principle the ATAC-sequencing libraries were prepared as in[73]. $5x10^4$ EmGFP-negative and EmGFP-positive TetOn-hESCs for four biological samples; TetOn-DUX4 in H1 clone 2, H1 clone 8, H9 clone 3 and H9 clone 4, were centrifuged at 500g for 5 min. The pellets were washed in cold 1X PBS by centrifugation at 500g for 5min. Each cell pellet was lysed in 50 µl of cold lysis buffer (10 mM Tris-HCl, pH 7.4; 10 mM NaCl, 3 mM $MgCl_2$, and 0.1% IGEPAL CA-630) and centrifuged at 500g

604 at 4°C for 10 min. The pellet was then resuspended in the transposase reaction mix
605 (2.5 µl of transposase in TD buffer) and incubated at 37°C for 30min. The reactions
606 were purified through columns and eluated in 20 µl. After addition of the barcode
607 oligos the DNA samples were amplified for 12 cycles (98°C for 10 seconds, 63°C for
608 30 seconds and 72°C for 60 seconds) in Phusion PCR master mix (Thermo Fisher
609 Scientific). The PCR products were purified through the columns and eluted in 20 µl.

610

611 *ATAC-seq data analysis*

612 Bcl files were converted and demultiplexed to fastq using the bcl2fastq program.
613 STAR[74] was used to index the human reference genome (hg19), obtained from
614 UCSC, and align the resulting fastq files. The resulting bam files with the mapped
615 reads were then converted to tag directories with subsequent peaks calling using the
616 HOMER suit of programs[48]. HOMER was also employed for counting the reads in the
617 identified peak regions. The raw tag counts from the peaks were then imported to
618 R/Bioconductor and differential peak analysis was performed using the edgeR
619 package and its general linear models pipeline. Peaks with an FDR adjusted p value
620 under 0.05 were termed significant. Plotting was done in R using packages Complex
621 heatmap, ggplot2 and ggbeeswarm. RepeatMasker table downloaded from UCSC
622 (http://hgdownload.soe.ucsc.edu/goldenPath/hg19/database/rmsk.txt.gz) was
623 converted to BED format and then intersected with the ATAC-seq peaks using the
624 intersectBed from BEDTools[46] to determine the peaks overlapped with ERVL-MaLR
625 elements. ATAC-seq data of human early embryo were obtained from GSE101571[30],
626 and scores around the ATAC-seq peaks were calculated with computeMatrix and

627 visualized with plotHeatmap from deepTools[47]. All the scripts and command line
628 options can be provided upon request.

629

630 *Immunocytochemistry of the human ESC*

631 The cells were fixed with 3.8% PFA, washed three times, permeabilised in 0.5% (v/v)
632 Tx100-PBS for 7 min, and washed with washing buffer (0.1% (v/v) Tween20-PBS).
633 The samples were incubated with ProteinBlock (Thermo Fisher Scientifi) at room
634 temperature for 10 min to prevent unspecific binding of primary antibody. Primary
635 antibody (rabbit MAb anti DUX4, clone E5-5, 1:400; Abcam) was diluted as
636 indicated in washing buffer and incubated at 4°C overnight. After washings,
637 fluorescence-conjugated secondary antibody (anti rabbit 594, A-21207; Thermo
638 Fisher Scientific) was diluted 1:1000 in washing buffer and incubated at room
639 temperature for 20 min. Nuclei were counterstained with DAPI 1:1000 in washing
640 buffer. The images were captured with Evos FL Cell Imaging system with 10X and
641 20X Plan Achromatic objectives.

642

643 *Immunocytochemistry of the human embryos*

644 The embryos were fixed in 3.8 % PFA at room temperature for 15min, washed three
645 times in the washing buffer (above), and permeabilised in 0.5 % Tx100-PBS at room
646 temperature for 15 min. Unspecific primary antibody binding was blocked as above.
647 DUX4 (as above) was incubated at 4°C overnight. The embryos were washed and
648 incubated in the secondary antibody (anti-rabbit 488, A-21202; Thermo Fisher
649 Scientific) diluted 1:500 in washing buffer (as above) at room temperature for 2

hours. After washings, nuclei were counterstained with DAPI 1:500 in washing buffer.

Imaging of the fixed human embryos

The embryos were imaged in washing buffer on Ibidi 8-well μ slides with Leica TCS SP8 confocal laser scanning microscope (Leica Microsystems, Mannheim, Germany) using Leica HC PL APO CS2 40X/1.10NA and Leica HC PL APO CS2 63X/1.20NA water objectives.

Confocal microscopy image analysis

Confocal images were processed using Fiji (http://fiji.sc). For the data presented in the Fig 1b, images were smoothened by Gaussian filter (radius=1 pixel kernel). For the quantification of the DUX4 intensity in the nucleus (Fig 1c), the DAPI channel was denoised using rolling ball (radius=100). The images were smoothened in 3D using Gaussian filter (radius=2 pixel kernel) and cell nuclei were segmented. The segmented regions were used to measure average pixel intensity per nucleus in each cell in the DUX4 channel. DUX4 intensity in the nucleus was normalized to intensity of the corresponding cytoplasmic DUX4 staining in the single representative plane.

Culture and microinjection of human embryos

Human triploid zygotes were warmed using Gems Warming Set (Genea Biomedx) and cultured in G-TL medium (Vitrolife) in 6 %O_2 and 6 % CO_2 at 37°C. 12 µl of either 20 µM scrambled control siRNA (AM4611, Thermo Fisher Scientific) or

673 DUX4-targeting siRNA (cat. 4457308, Thermo Fisher Scientific) diluted in
674 nucleotide-free H_2O were mixed with total of 500 ng of GAP-GFP mRNA and
675 centrifuged at maximum speed at 4°C for 10 min. The embryos were microinjected
676 using Eppendorf microinjector and placed in G-TL medium in Geri dish for 3D time-
677 lapse imaging (Geri incubator, Genea Biomedx, Australia).

678

679 *Human embryo live imaging*

680 Imaging of the human triploid embryos was initiated immediately after
681 microinjections (Geri incubator). Images were captured in 3D every 15 minutes until
682 the embryos were removed for fluorescence staining or termination of the experiment.

683

684 *Ethical approvals*

685 Collection and experiments on human oocytes and embryos were approved by the
686 Helsinki University Hospital ethical committee, diary numbers 308/13/03/03/2015
687 and HUS/1069/2016. Human surplus oocytes, zygotes, and embryos were donated by
688 couples that had undergone infertility treatments at Helsinki University Hospital
689 Reproduction Medicine Unit. The donations were done with an informed consent and
690 patients understood that donating oocytes, zygotes, or embryos is voluntary.

691

692 *Acknowledgements*

693 We are grateful for all the couples that donated their surplus oocytes, zygotes, or
694 embryos for this project. We thank the IVF nurses at Helsinki University Hospital

Reproductive Medicine Unit for recruiting the couples for oocyte and embryo donation program, Dr. Diego Balboa-Alonso for the pB-ires-EmGFP-pA-PGK-Puro plasmid and discussions of the data and Dr. Jere Weltner for helpful discussions. We acknowledge Biomedicum Imaging Unit (Helsinki), Functional Genomics Unit (Helsinki), Biomedicum Flow Cytometry Unit (Helsinki), Bioinformatics and Expression Analysis Core Facility (Stockholm) for skilled technical assistance. We thank Dr. Jukka Lehtonen for scientific IT support (Biocenter Finland) and CSC IT Center for Science for supercomputing. We thank prof. Outi Hovatta for inspiration and introducing the senior author to the field of early embryogenesis. This study is based on collaboration between the groups of the last seven authors. This project was supported by Jane and Aatos Erkko foundation, Sigrid Jusélius foundation, Finnish Academy, and Helsinki University Hospital funds. SV was supported by Jane and Aatos Erkko foundation. MY was supported by the Scandinavia-Japan Sasakawa Foundation, the Japan Eye Bank Association, the Astellas Foundation for Research on Metabolic Disorders, and the Japan Society for the Promotion of Science Overseas Research Fellowships. MT was supported by Joe, Pentti and Tor Memorial Foundation, Graduate School of Åbo Akademi University. VR was supported by Foundation of Åbo Akademi University and Magnus Ehrnrooth Foundation.

Contributions

SV, SK and JK conceived and coordinated the study. YM, TRB, MV, MSJ, TT, SK and JK supervised the work in each contributing laboratory. Every author participated in either planning or conducting respective experiments and analyzing or interpreting the data. SV, MY, LG, VR, TA, MT, MSJ, JK wrote the manuscript. All authors approved the final version of the manuscript.

720

721 *Competing interests*

722 The authors declare no competing interests.

723

724

Figure Legends

Figure 1. DUX4 expression in human embryos.

(a) Log_2 RPM of DUX4 mRNA reads in human oocytes (N=20), zygotes (N=59), 2-cell (N=4), 4-cell (N=14), and 8-cell (N=15) embryos.

(b) Representative confocal images of zygotes (N=3), 2-cell (N=3), 4-cell (N=4), and 8-cell (N=2) human embryos stained with monoclonal DUX4 antibody E5-5 (green). Nuclei counterstained with DAPI (magenta).

(c) 3D quantification of DUX4 intensity in the nuclei of the human embryos, normalised to cytoplasmic DUX4 staining (single plane) with standard deviation.

Figure 2. Structural features of DUX4.

(a) Domain structure of full-length DUX4: N- and C-terminal amino acid residues, as well as boundary residues for the homeodomains HD1 and HD2, three predicted ordered C-terminal regions (disorder value < 0.5; red curve) and 9aaTAD motif (blue). Conservation of residues in primates versus the human sequence C-terminal to residue G153 (green curve) and sequence alignment and predicted secondary structures (alpha helices) of the ordered regions. Residue numbering from UniProt ID Q9UBX2.

(b) Crystal structure (PDB:6E8C; Lee et al., 2018) of DUX4 HD1 (blue) and HD2 (gold) in complex with the consensus DNA motif "TAATCTAATCA" (grey). Disordered/linker regions, magenta; residues forming inter-homeodomain contacts drawn as sticks.

747 **(c)** Structure of DUX4 HD1 (blue) and 2 (gold) without DNA. The coordinates of the
748 bound DNA of the X-ray structure shown in (b) were deleted from the coordinate file
749 of DUX4 structure. Coloring as in (b).

750 **(d)** View focused on the inter-homeodomain interactions shown in (c). Hydrogen
751 bonds, yellow dash lines; coloring as in (b).

752 **(e)** Sequence comparison of residues forming inter-homeodomain contacts.
753 **(f)** Root-mean-squared fluctuations (RMSF) of the C α atoms of the X-ray structure
754 of DUX4 with (red curve) and without (blue curve) bound DNA during a 100 ns MD
755 simulation. HD1 (blue), linker (magenta) and HD2 (gold).

756 **(g)** Root-mean-squared deviation (RMSD) of the backbone atoms of the X-ray
757 structure of DUX4 with and without bound DNA during a 100 ns MD simulation.
758 Homedomains with (HD1-HD2 +DNA) and without (HD1-HD2) bound DNA and
759 single homedomains (HD1+DNA and HD2 +DNA) with bound DNA were used in
760 the simulations.

761

762 **Figure 3. The protein – protein interaction network of DUX4.**

763 **(a)** High confidence protein-protein interactions detected by AP-MS (n=24) and
764 BioID (n=139) -methods (SAINT score > 0.74). Average spectral count of the
765 interaction filtered to show interactions larger than the median (AP-MS=4.125,
766 BioID=7.5).
767 **(b)** DUX4 interactome, filtered to show spectral counts larger than median. BioID -
768 interactions shown in red lines and AP-MS -interactions in blue, if protein appeared in
769 both data sets it is outlined in bold black. Known prey-prey interactions shown in grey
770 (iREF).

Figure 4. Knockdown of DUX4 in human embryos.

(a) Schematic of the experimental set up.

(b) Human embryos immunostained with DUX4 antibody (green) 24 h after microinjection with either control siRNA (left panel) or DUX4 targeting siRNA (right panel). Nuclei counterstained with DAPI (blue). Overlay of a single representative z plane and the corresponding z-planes shown for DUX4 staining, nucleus and bright field channels on the right side of each overlay. Scale bar 50 μm.
(c) Scatter plot of the expression levels of TFEs across the siCTRL and siDUX4 embryos. Red dots represent significantly upregulated TFEs by siDUX4 and grey crosses represent TFEs, which showed no significant change.
(d-f) TFEs upregulated (red dots) or showing no significant change (grey crosses) by siDUX4 in the human OET transcriptome as in[3]. Comparisons in d: oocyte to 4-cell, e: zygote to 4-cell, and f: 4-cell to 8-cell. The dotted line marks the cell division effect on cellular RNA content. *P*-values were calculated with Fisher's exact test for the frequency of the siDUX4-upregulated TFEs of the TFEs normally downregulated during respective stages.

(g) Expression levels of the oocyte-specific genes in siCTRL and siDUX4 embryos. Asterisks represent statistical significance (q-value < 0.05). Horizontal lines represent the median values in each group.

Figure 5. Transcriptome and ChIP-seq analysis on the TetOn-DUX4 hESCs.
(a) Schematic of the experimental set up.

794 **(b)** Doxicycline induction of TetOn-DUX4 hESCs induces expression of DUX4 and
795 DUX4 target genes, ZSCAN4 and TRIM48. Shown for H1-TetOn-DUX4 clone 2. All
796 clones selected for experiments followed the same trend. X-axis indicates time (h)
797 incubated in doxycycline. Relative mRNA expression levels were normalized to the
798 non-induced cells.

799 **(c)** 4-hour doxycycline induction upregulates DUX4 protein expression in the
800 nucleus, shown for H1-TetOn-DUX4 clone 2.

801 **(d)** Proportion of the upregulated and downregulated TFEs based on the genome
802 annotation.

803 **(e)** Expression level of putative DUX4 target genes. Asterisks represent statistical
804 significance (q-value < 0.05). Horizontal lines represent the median values in each
805 group.

806 **(f)** Proportion of the upregulated (Up), downregulated (Down), and non-significantly
807 changed (NS) TFEs by DUX4 induction among the minor (Oocyte to 4-cell embryo)
808 and major (4- to 8-cell embryo) EGA genes. One TFE out of the 129 major EGA
809 genes annotated on unassigned chromosome (ChrUn) and was excluded from the
810 analysis.

811 **(g)** DUX4 ChIP-seq intensity[26] around the peaks of reads within the upregulated TFEs
812 (blue) and all the detected TFEs (green).

813 **(h)** De novo motif enrichment analysis of the DUX4-induced TFEs. Top: the most
814 significantly enriched motif (P = 1e-961). Bottom: the best-matched known motif
815 (DUX4 ChIP-seq of myoblasts: GSE75791[29]; matched score = 0.92).

816 **(i)** Enrichment analysis of the DUX4-induced TFEs with publicly available ChIP-seq
817 datasets. A total of 7,216 ChIP-seq data for transcription factors are shown. ChIP-seq

818 data for DUX4 are shown in red. Dots on the left side of the dashed line are
819 underrepresented, whereas dots on the right side are overrepresented.

820

821 **Figure 6. Novel DUX4 targets.**

822 **(a)** Predicted *KHDC1* pseudogene 1 (clone K5.2), at chromosome 6 (73,918,461-
823 73,920,115) was expressed by the human 4-cell embryos (FE463525) and upregulated
824 in the TetOn -DUX4- hESCs (TFE93242). TFEs overlapped with DUX4 binding sites
825 (DUX4 ChIP). cDNA clone K5.2 (thick orange regions indicate exons and grey thin
826 regions indicate introns) corresponded to the *KHDC1* pseudogene 1 transcript
827 assembly in TetOn-DUX4 cells. Transcript assemblies (mRNA Genbank and human
828 ESTs), including unspliced, are shown.

829 **(b)** Putative RING-finger type E3 ubiquitin ligase at chromosome 2 (108,273,771-
830 108,277,850) was expressed by the human 4-cell embryos (FE130507) and it was
831 upregulated in the TetOn-DUX4 hESCs (TFE25640). DUX4 ChIP-seq peak
832 overlapped with the TFEs. RET11.1 was cloned from human 4-cell embryo (clone
833 RET11.1). Thick blue regions indicate exons and thin grey regions indicate introns.
834 Transcript assemblies (mRNA Genbank and human ESTs), including unspliced, are
835 shown.

836 **(c)** Putative RING-finger domain protein at chromosome 8 (210,701-215,100) was
837 expressed by the human 4-cell embryos (TFE533694) and induced by TetOn-DUX4
838 hESCs (TFE102707). ChIP-seq overlapped with the TFEs. Two cDNA clones, Ring
839 4.2 and Ring 10.22, were expressed in the human 4-cell embyos. Thick blue regions
840 indicate exons and grey thin regions indicate introns. Transcript assemblies (mRNA
841 Genbank and human ESTs), including unspliced, are shown.

Figure 7. Integrated analysis of the DUX4 induced changes in the chromatin and transcriptome of the hESCs.

(a) Heatmap of the 4,686 ATAC-sequencing reads across all samples at ATAC-seq peaks that overlap with differentially regulated TFE reads. Counts for each peak were standardized across each sample (mean=0, sd=1). Samples and peaks were then clustered using hierarchical clustering. The Separate heatmap of the ATAC-seq shows if the changes in the heatmap are significant (red: ATAC-reg gained; blue: ATAC-reg lost; grey: ATAC-reg non-significant). TFE-Reg heatmap shows if the overlapping TFE site is upregulated or downregulated (red: upregulated; blue: downregulated). **(b)** Quasi random plot showing the results of the differential peak analysis on the ATAC-seq and STRT-RNA-seq. Each point is an ATAC-seq peak. Analyses were carried out on peaks that were repeated at least three times. Red: ATAC-seq gained; blue: ATAC-seq lost; grey: ATAC-seq non-significant. Y-axis: The log fold change of the ATAC-seq reads in the DUX4 expressing versus the control samples. X-axis: The ATAC-seq peaks overlapping either with the down-regulated TFEs or upregulated TFEs.

(c) Density plot showing distribution of the ATAC-seq peaks relative to the TSS of genes separated by how the peak is regulated by the DUX4-expression. red: ATAC-reg gained; blue: ATAC-reg lost; grey: ATAC-reg non-significant.

(d) Proportion of the peaks overlapped with ERVL-MaLR elements in the gained, non-significant and lost ATAC-reg peaks (pink) by DUX4 induction. Inset pie charts inidicate the proportion of the ATAC-gained peaks overlapping with DUX4 binding sites (green).

866 **(e)** ATAC-reg intensity of human early embryo[30] around the gained, non-significant
867 (NS), and lost ATAC-reg peaks by DUX4 induction which overlap with ERVL-
868 MaLR elements.

869

870

References

1 Jukam, D., Shariati, S. A. M. & Skotheim, J. M. Zygotic Genome Activation in Vertebrates. *Developmental cell* **42**, 316-332, doi:10.1016/j.devcel.2017.07.026 (2017).

2 Braude, P., Bolton, V. & Moore, S. Human gene expression first occurs between the four- and eight-cell stages of preimplantation development. *Nature* **332**, 459-461, doi:10.1038/332459a0 (1988).

3 Tohonen, V. *et al.* Novel PRD-like homeodomain transcription factors and retrotransposon elements in early human development. *Nature communications* **6**, 8207, doi:10.1038/ncomms9207 (2015).

4 Blakeley, P. *et al.* Defining the three cell lineages of the human blastocyst by single-cell RNA-seq. *Development* **142**, 3613, doi:10.1242/dev.131235 (2015).

5 Galan, A. *et al.* Functional genomics of 5- to 8-cell stage human embryos by blastomere single-cell cDNA analysis. *PloS one* **5**, e13615, doi:10.1371/journal.pone.0013615 (2010).

6 Stirparo, G. G. *et al.* Integrated analysis of single-cell embryo data yields a unified transcriptome signature for the human pre-implantation epiblast. *Development* **145**, doi:10.1242/dev.158501 (2018).

7 Boroviak, T. *et al.* Single cell transcriptome analysis of human, marmoset and mouse embryos reveals common and divergent features of preimplantation development. *Development* **145**, doi:10.1242/dev.167833 (2018).

8 De Iaco, A. *et al.* DUX-family transcription factors regulate zygotic genome activation in placental mammals. *Nat Genet* **49**, 941-945, doi:10.1038/ng.3858 (2017).

9 Hendrickson, P. G. *et al.* Conserved roles of mouse DUX and human DUX4 in activating cleavage-stage genes and MERVL/HERVL retrotransposons. *Nature genetics* **49**, 925-934, doi:10.1038/ng.3844 (2017).

10 Tohonen, V. *et al.* Transcriptional activation of early human development suggests DUX4 as an embryonic regulator. doi:https://doi.org/10.1101/123208 (2017).

11 Yan, L. *et al.* Single-cell RNA-Seq profiling of human preimplantation embryos and embryonic stem cells. *Nature structural & molecular biology* **20**, 1131-1139, doi:10.1038/nsmb.2660 (2013).

12 Dang, Y. *et al.* Tracing the expression of circular RNAs in human pre-implantation embryos. *Genome biology* **17**, 130, doi:10.1186/s13059-016-0991-3 (2016).

13 Xue, Z. *et al.* Genetic programs in human and mouse early embryos revealed by single-cell RNA sequencing. *Nature* **500**, 593-597, doi:10.1038/nature12364 (2013).

14 Whiddon, J. L., Langford, A. T., Wong, C. J., Zhong, J. W. & Tapscott, S. J. Conservation and innovation in the DUX4-family gene network. *Nat Genet* **49**, 935-940, doi:10.1038/ng.3846 (2017).

15 Codutti, L. *et al.* The solution structure of DNA-free Pax-8 paired box domain accounts for redox regulation of transcriptional activity in the pax protein family. *The Journal of biological chemistry* **283**, 33321-33328, doi:10.1074/jbc.M805717200 (2008).

16 Mitsuhashi, H. *et al.* Functional domains of the FSHD-associated DUX4 protein. *Biology open* **7**, doi:10.1242/bio.033977 (2018).

17 Katayama, S. *et al.* Phylogenetic and mutational analyses of human LEUTX, a homeobox gene implicated in embryogenesis. *Scientific reports* **8**, 17421, doi:10.1038/s41598-018-35547-5 (2018).

18 Goto, N. K., Zor, T., Martinez-Yamout, M., Dyson, H. J. & Wright, P. E. Cooperativity in transcription factor binding to the coactivator CREB-binding protein (CBP). The mixed lineage leukemia protein (MLL) activation domain binds to an allosteric site on the KIX domain. *The Journal of biological chemistry* **277**, 43168-43174, doi:10.1074/jbc.M207660200 (2002).

19 Lee, J. K. *et al.* Crystal Structure of the Double Homeodomain of DUX4 in Complex with DNA. *Cell reports* **25**, 2955-2962 e2953, doi:10.1016/j.celrep.2018.11.060 (2018).

20 Varjosalo, M. *et al.* Interlaboratory reproducibility of large-scale human protein-complex analysis by standardized AP-MS. *Nature methods* **10**, 307-314, doi:10.1038/nmeth.2400 (2013).

21 Liu, X. *et al.* An AP-MS- and BioID-compatible MAC-tag enables comprehensive mapping of protein interactions and subcellular localizations. *Nature communications* **9**, 1188, doi:10.1038/s41467-018-03523-2 (2018).

22 Islam, S. *et al.* Highly multiplexed and strand-specific single-cell RNA 5' end sequencing. *Nature protocols* **7**, 813-828, doi:10.1038/nprot.2012.022 (2012).

23 Krjutskov, K. *et al.* Single-cell transcriptome analysis of endometrial tissue. *Human reproduction* **31**, 844-853, doi:10.1093/humrep/dew008 (2016).

24 Komljenovic, A., Roux, J., Wollbrett, J., Robinson-Rechavi, M. & Bastian, F. B. BgeeDB, an R package for retrieval of curated expression datasets and for gene list expression localization enrichment tests. *F1000Research* **5**, 2748, doi:10.12688/f1000research.9973.2 (2016).

25 Dandapat, A., Hartweck, L. M., Bosnakovski, D. & Kyba, M. Expression of the human FSHD-linked DUX4 gene induces neurogenesis during differentiation of murine embryonic stem cells. *Stem cells and development* **22**, 2440-2448, doi:10.1089/scd.2012.0643 (2013).

26 Geng, L. N. *et al.* DUX4 activates germline genes, retroelements, and immune mediators: implications for facioscapulohumeral dystrophy. *Developmental cell* **22**, 38-51, doi:10.1016/j.devcel.2011.11.013 (2012).

27 Young, J. M. *et al.* DUX4 binding to retroelements creates promoters that are active in FSHD muscle and testis. *PLoS genetics* **9**, e1003947, doi:10.1371/journal.pgen.1003947 (2013).

28 Jouhilahti, E. M. *et al.* The human PRD-like homeobox gene LEUTX has a central role in embryo genome activation. *Development* **143**, 3459-3469, doi:10.1242/dev.134510 (2016).

29 Eidahl, J. O. *et al.* Mouse Dux is myotoxic and shares partial functional homology with its human paralog DUX4. *Human molecular genetics* **25**, 4577-4589, doi:10.1093/hmg/ddw287 (2016).

30 Wu, J. *et al.* Chromatin analysis in human early development reveals epigenetic transition during ZGA. *Nature* **557**, 256-260, doi:10.1038/s41586-018-0080-8 (2018).

31 Tadros, W. & Lipshitz, H. D. The maternal-to-zygotic transition: a play in two acts. *Development* **136**, 3033-3042, doi:10.1242/dev.033183 (2009).

32 Walser, C. B. & Lipshitz, H. D. Transcript clearance during the maternal-to-zygotic transition. *Current opinion in genetics & development* **21**, 431-443, doi:10.1016/j.gde.2011.03.003 (2011).

33 Lee, M. T., Bonneau, A. R. & Giraldez, A. J. Zygotic genome activation during the maternal-to-zygotic transition. *Annual review of cell and developmental biology* **30**, 581-613, doi:10.1146/annurev-cellbio-100913-013027 (2014).

34 Winata, C. L. *et al.* Cytoplasmic polyadenylation-mediated translational control of maternal mRNAs directs maternal-to-zygotic transition. *Development* **145**, doi:10.1242/dev.159566 (2018).

35 Suzumori, N., Burns, K. H., Yan, W. & Matzuk, M. M. RFPL4 interacts with oocyte proteins of the ubiquitin-proteasome degradation pathway. *Proceedings of the National Academy of Sciences of the United States of America* **100**, 550-555, doi:10.1073/pnas.0234474100 (2003).

36 Rajkovic, A., Lee, J. H., Yan, C. & Matzuk, M. M. The ret finger protein-like 4 gene, Rfpl4, encodes a putative E3 ubiquitin-protein ligase expressed in adult germ cells. *Mechanisms of development* **112**, 173-177 (2002).

37 Yang, Y. *et al.* The E3 ubiquitin ligase RNF114 and TAB1 degradation are required for maternal-to-zygotic transition. *EMBO reports* **18**, 205-216, doi:10.15252/embr.201642573 (2017).

38 Chen, Z. & Zhang, Y. Loss of DUX causes minor defects in zygotic genome activation and is compatible with mouse development. *Nat Genet* **51**, 947-951, doi:10.1038/s41588-019-0418-7 (2019).

39 De Iaco, A., Verp S., Offner S., Trono D. DUX is a non-essential synchronizer of zygotic genome activation. doi:https://doi.org/10.1101/569434 (2019).

40 Madissoon, E. *et al.* Pleomorphic Adenoma Gene 1 Is Needed For Timely Zygotic Genome Activation and Early Embryo Development. *Scientific reports* **9**, 8411, doi:10.1038/s41598-019-44882-0 (2019).

41 Kruse K., D. N., Enriquez-Gasca R., Gaume X., Torres-Padilla M-E., Vaquerizas JM. Transposable elements drive reorganisation of 3D chromatin during early embryogenesis. doi:https://doi.org/10.1101/523712 (2019).

42 Franke, V. *et al.* Long terminal repeats power evolution of genes and gene expression programs in mammalian oocytes and zygotes. *Genome research* **27**, 1384-1394, doi:10.1101/gr.216150.116 (2017).

43 Liu, L. *et al.* An integrated chromatin accessibility and transcriptome landscape of human pre-implantation embryos. *Nature communications* **10**, 364, doi:10.1038/s41467-018-08244-0 (2019).

44 Islam, S. *et al.* Quantitative single-cell RNA-seq with unique molecular identifiers. *Nature methods* **11**, 163-166, doi:10.1038/nmeth.2772 (2014).

45 Katayama, S., Tohonen, V., Linnarsson, S. & Kere, J. SAMstrt: statistical test for differential expression in single-cell transcriptome with spike-in normalization. *Bioinformatics* **29**, 2943-2945, doi:10.1093/bioinformatics/btt511 (2013).

46 Quinlan, A. R. & Hall, I. M. BEDTools: a flexible suite of utilities for comparing genomic features. *Bioinformatics* **26**, 841-842, doi:10.1093/bioinformatics/btq033 (2010).

47 Ramirez, F., Dundar, F., Diehl, S., Gruning, B. A. & Manke, T. deepTools: a flexible platform for exploring deep-sequencing data. *Nucleic acids research* **42**, W187-191, doi:10.1093/nar/gku365 (2014).

48 Heinz, S. *et al.* Simple combinations of lineage-determining transcription factors prime cis-regulatory elements required for macrophage and B cell identities. *Molecular cell* **38**, 576-589, doi:10.1016/j.molcel.2010.05.004 (2010).

49 Oki, S. *et al.* ChIP-Atlas: a data-mining suite powered by full integration of public ChIP-seq data. *EMBO reports* **19**, doi:10.15252/embr.201846255 (2018).

50 Tang, F. *et al.* RNA-Seq analysis to capture the transcriptome landscape of a single cell. *Nature protocols* **5**, 516-535, doi:10.1038/nprot.2009.236 (2010).

51 Johnson, M. *et al.* NCBI BLAST: a better web interface. *Nucleic acids research* **36**, W5-9, doi:10.1093/nar/gkn201 (2008).

52 Katoh, K. & Standley, D. M. MAFFT multiple sequence alignment software version 7: improvements in performance and usability. *Molecular biology and evolution* **30**, 772-780, doi:10.1093/molbev/mst010 (2013).

53 Porollo, A. A., Adamczak, R. & Meller, J. POLYVIEW: a flexible visualization tool for structural and functional annotations of proteins. *Bioinformatics* **20**, 2460-2462, doi:10.1093/bioinformatics/bth248 (2004).

54 Adamczak, R., Porollo, A. & Meller, J. Accurate prediction of solvent accessibility using neural networks-based regression. *Proteins* **56**, 753-767, doi:10.1002/prot.20176 (2004).

55 Magnan, C. N. & Baldi, P. SSpro/ACCpro 5: almost perfect prediction of protein secondary structure and relative solvent accessibility using profiles, machine learning and structural similarity. *Bioinformatics* **30**, 2592-2597, doi:10.1093/bioinformatics/btu352 (2014).

56 Wang, S., Li, W., Liu, S. & Xu, J. RaptorX-Property: a web server for protein structure property prediction. *Nucleic acids research* **44**, W430-435, doi:10.1093/nar/gkw306 (2016).

57 Piskacek, S. *et al.* Nine-amino-acid transactivation domain: establishment and prediction utilities. *Genomics* **89**, 756-768, doi:10.1016/j.ygeno.2007.02.003 (2007).

58 Berman, H. M. *et al.* The Protein Data Bank. *Nucleic acids research* **28**, 235-242, doi:10.1093/nar/28.1.235 (2000).

59 Lehtonen, J. V. *et al.* BODIL: a molecular modeling environment for structure-function analysis and drug design. *Journal of computer-aided molecular design* **18**, 401-419 (2004).

60 Case, D. *et al.* AMBER 2018. (2018).

61 Maier, J. A. *et al.* ff14SB: Improving the Accuracy of Protein Side Chain and Backbone Parameters from ff99SB. *Journal of chemical theory and computation* **11**, 3696-3713, doi:10.1021/acs.jctc.5b00255 (2015).

62 Zgarbova, M. *et al.* Refinement of the Sugar-Phosphate Backbone Torsion Beta for AMBER Force Fields Improves the Description of Z- and B-DNA. *Journal of chemical theory and computation* **11**, 5723-5736, doi:10.1021/acs.jctc.5b00716 (2015).

63 Jorgensen, W., Chandrasekhar, J. & Madura, J. Comparison of simple potential functions for simulating liquid water. *The Journal of chemical physics* **79**, doi: https://doi.org/10.1063/1.445869 (1983).

64 Essmann, U. *et al.* A smooth particle mesh Ewald method. *The Journal of chemical physics* **103**, 8577-8593, doi:10.1063/1.470117 (1995).

65 Berendsen, H. J. C., Postma, J. P., van Gunsteren, A., DiNola, A. & J.R., H. Molecular dynamics with coupling to an external bath. *The Journal of chemical physics* **81**, doi:https://doi.org/10.1063/1.448118 (1984).

66 Roe, D. R. & Cheatham, T. E., 3rd. PTRAJ and CPPTRAJ: Software for Processing and Analysis of Molecular Dynamics Trajectory Data. *Journal of chemical theory and computation* **9**, 3084-3095, doi:10.1021/ct400341p (2013).

67 Humphrey, W., Dalke, A. & Schulten, K. VMD: visual molecular dynamics. *Journal of molecular graphics* **14**, 33-38, 27-38 (1996).

68 Choi, H. *et al.* SAINT: probabilistic scoring of affinity purification-mass spectrometry data. *Nature methods* **8**, 70-73, doi:10.1038/nmeth.1541 (2011).

69 Mellacheruvu, D. *et al.* The CRAPome: a contaminant repository for affinity purification-mass spectrometry data. *Nature methods* **10**, 730-736, doi:10.1038/nmeth.2557 (2013).

70 Wang, J., Vasaikar, S., Shi, Z., Greer, M. & Zhang, B. WebGestalt 2017: a more comprehensive, powerful, flexible and interactive gene set enrichment analysis toolkit. *Nucleic acids research* **45**, W130-W137, doi:10.1093/nar/gkx356 (2017).

71 Meldal, B. H. *et al.* The complex portal--an encyclopaedia of macromolecular complexes. *Nucleic acids research* **43**, D479-484, doi:10.1093/nar/gku975 (2015).

72 Giurgiu, M. *et al.* CORUM: the comprehensive resource of mammalian protein complexes-2019. *Nucleic acids research* **47**, D559-D563, doi:10.1093/nar/gky973 (2019).

73 Buenrostro, J. D., Wu, B., Chang, H. Y. & Greenleaf, W. J. ATAC-seq: A Method for Assaying Chromatin Accessibility Genome-Wide. *Current protocols in molecular biology* **109**, 21 29 21-29, doi:10.1002/0471142727.mb2129s109 (2015).

74 Dobin, A. *et al.* STAR: ultrafast universal RNA-seq aligner. *Bioinformatics* **29**, 15-21, doi:10.1093/bioinformatics/bts635 (2013).

Fig.1

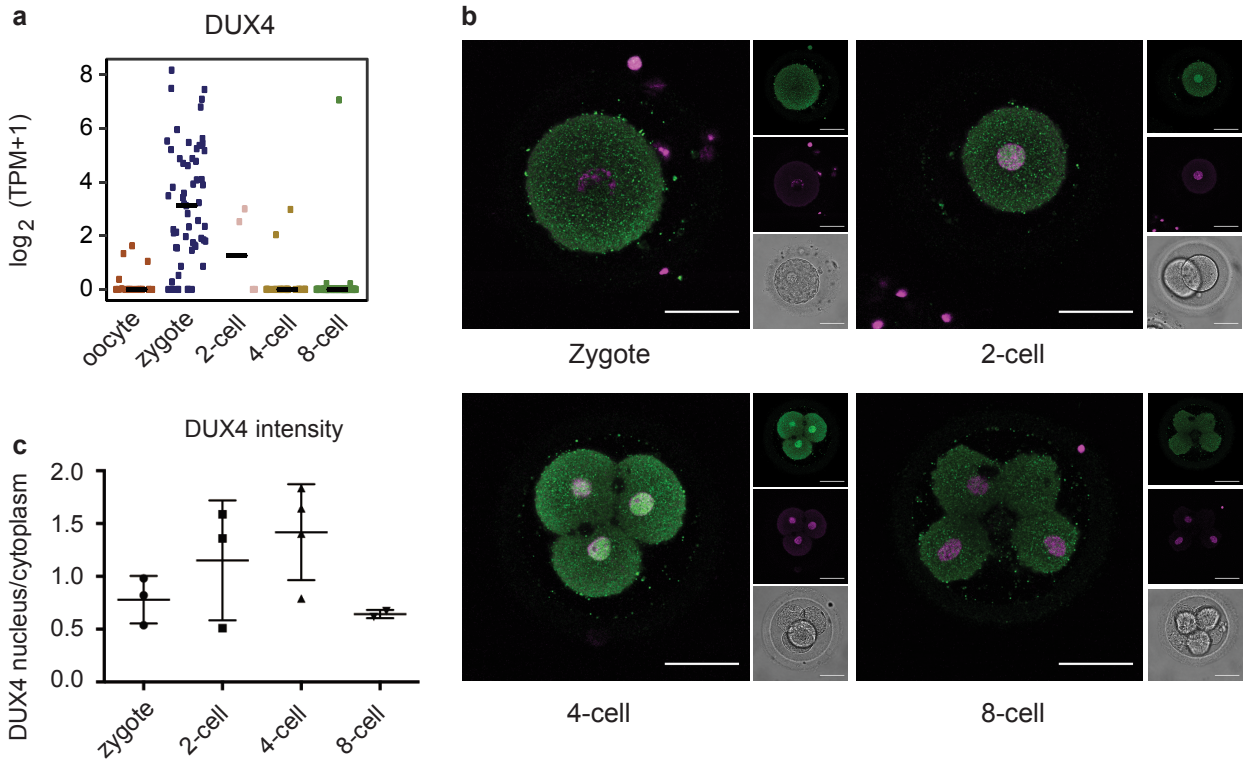

Fig. 2

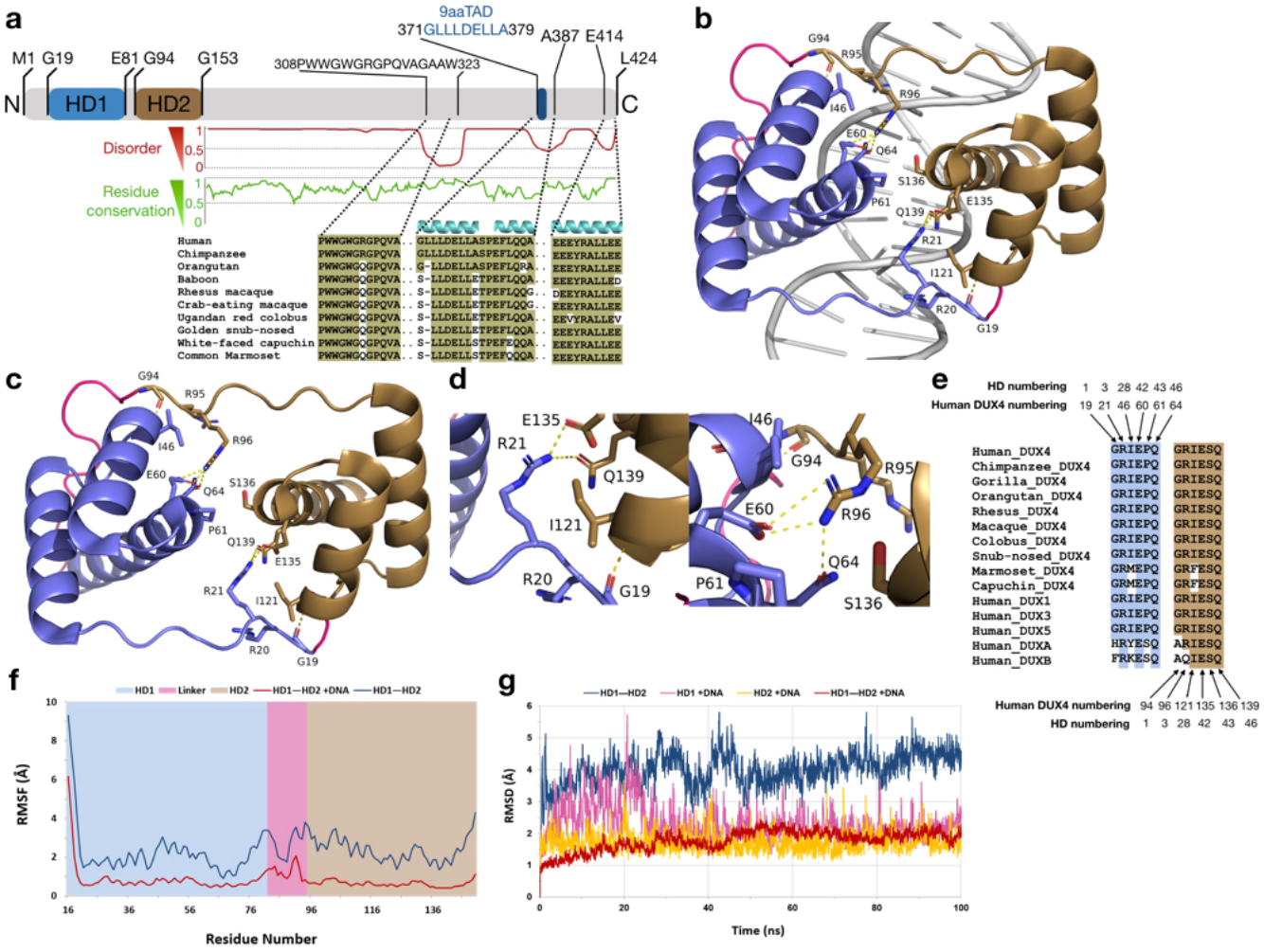

Fig.3

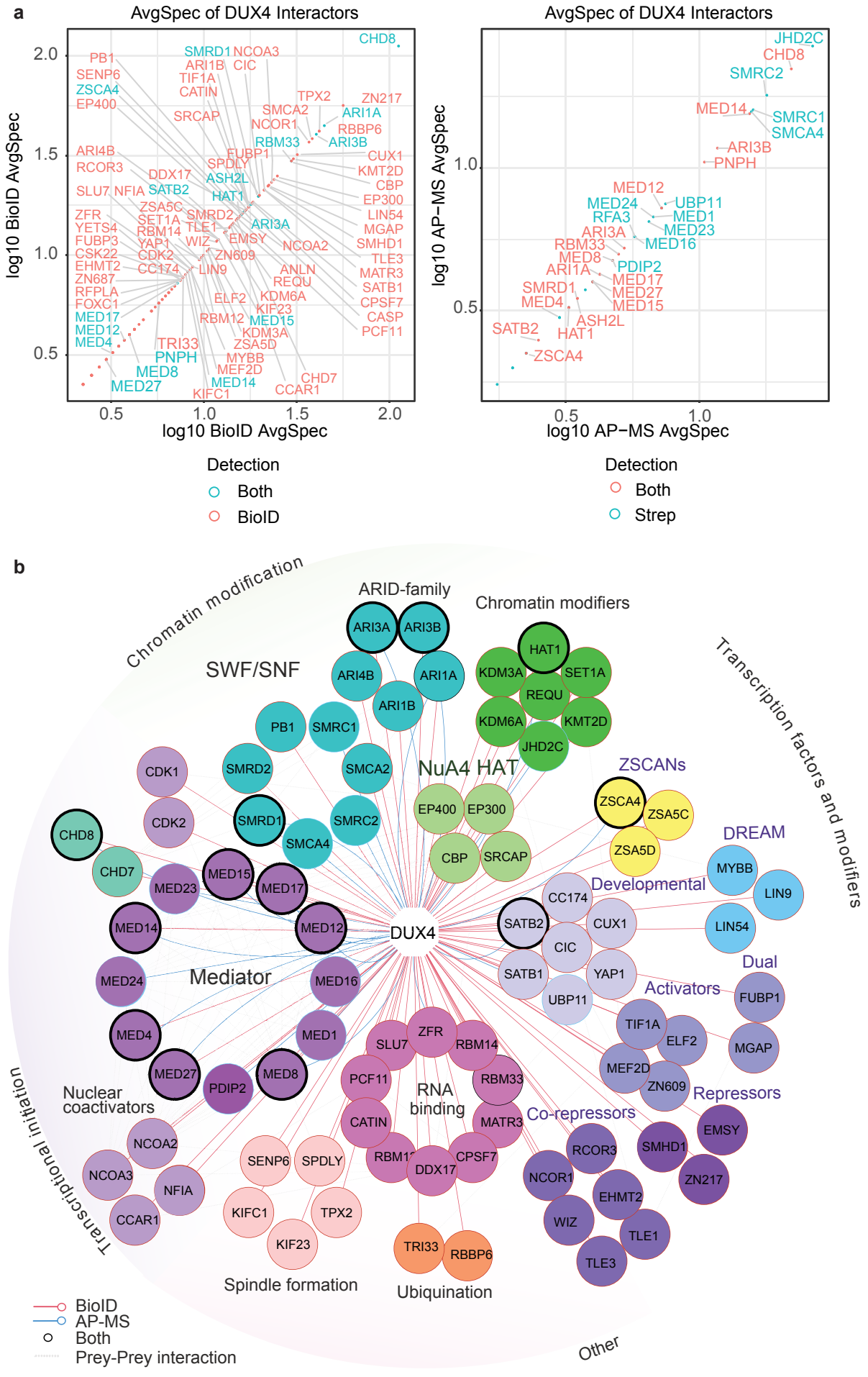

Fig. 4

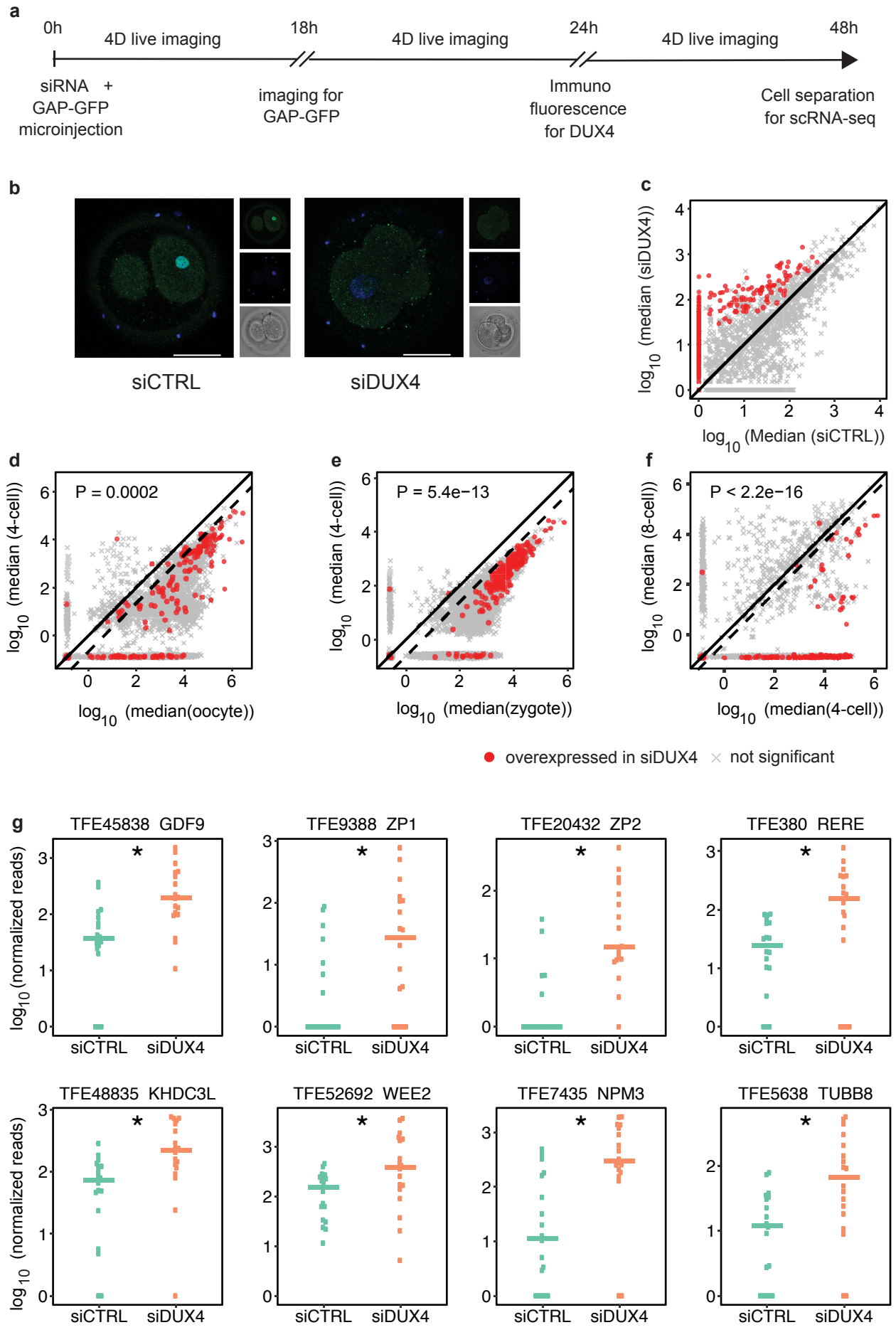

Fig. 5

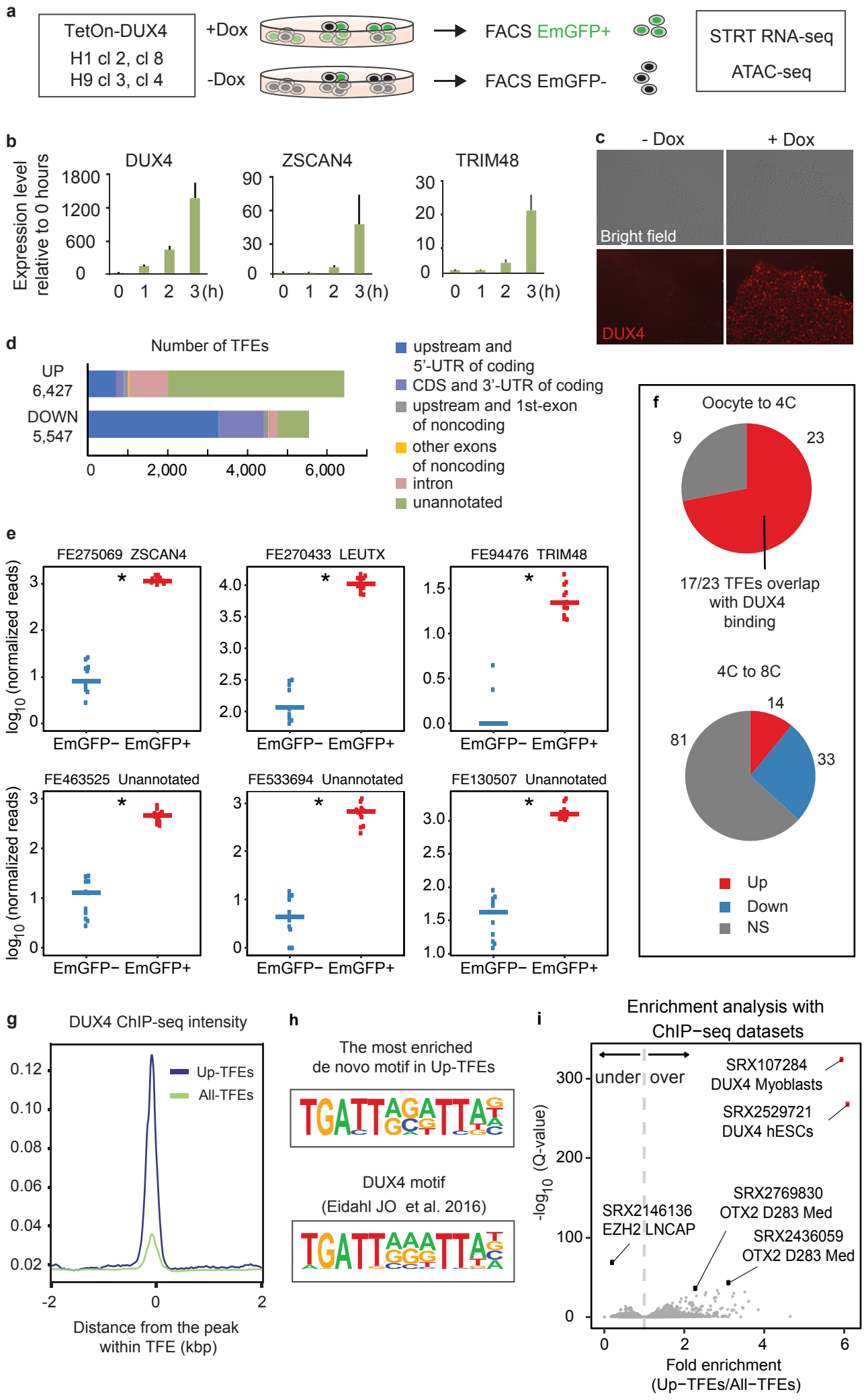

Fig. 6

a

KHDC1 pseudo gene 1
ENA accession LR694084, LR694085

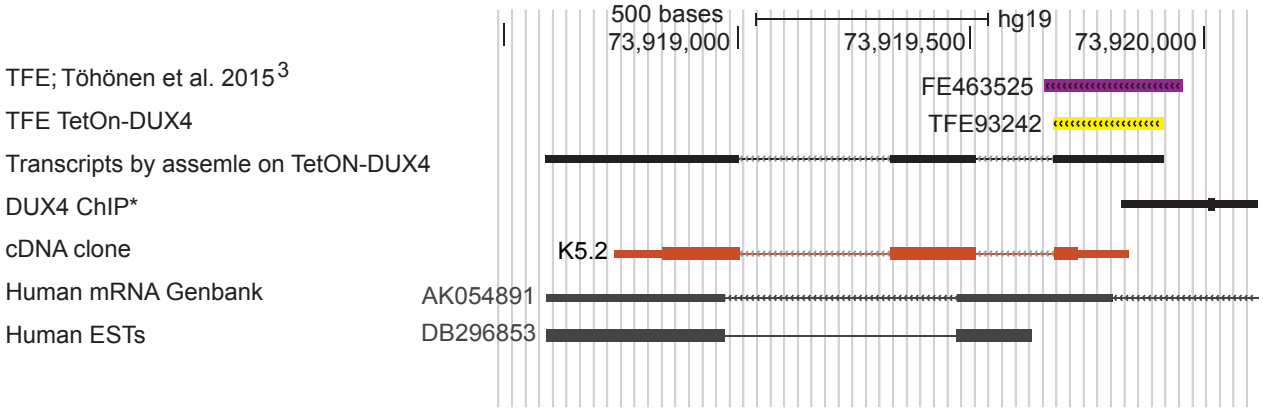

b

RING-finger type E3 ubiquitin ligase
ENA accession LR694082, LR694083

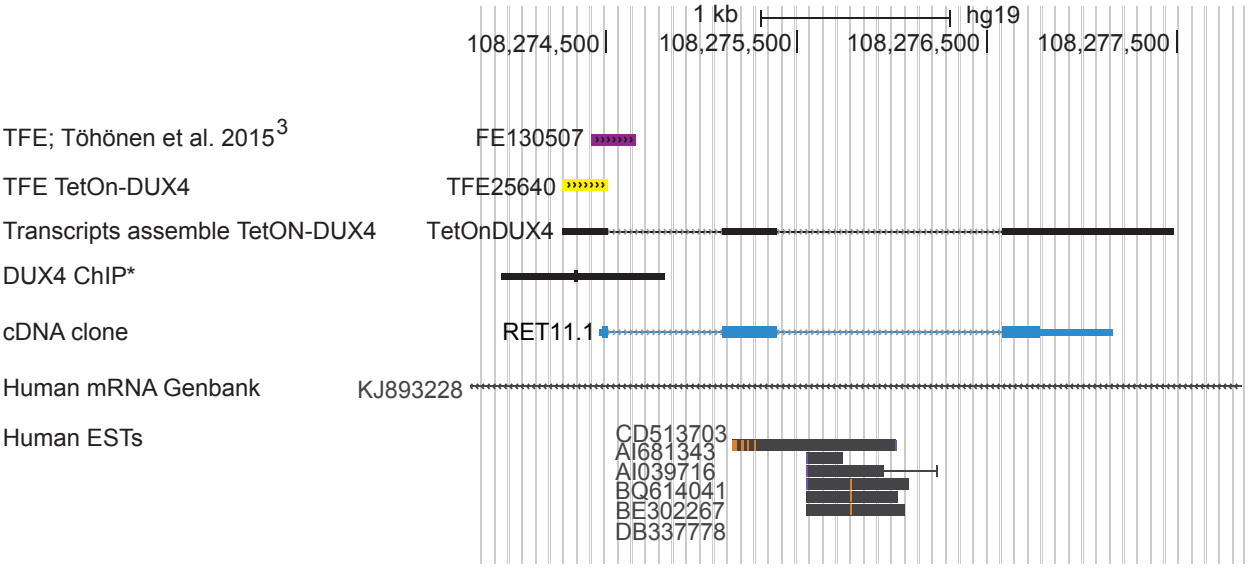

c

RING-finger domain protein
ENA accession:
LR694086, LR694087 (Ring10.2)
LR694088, LR694089 (Ring4.2)

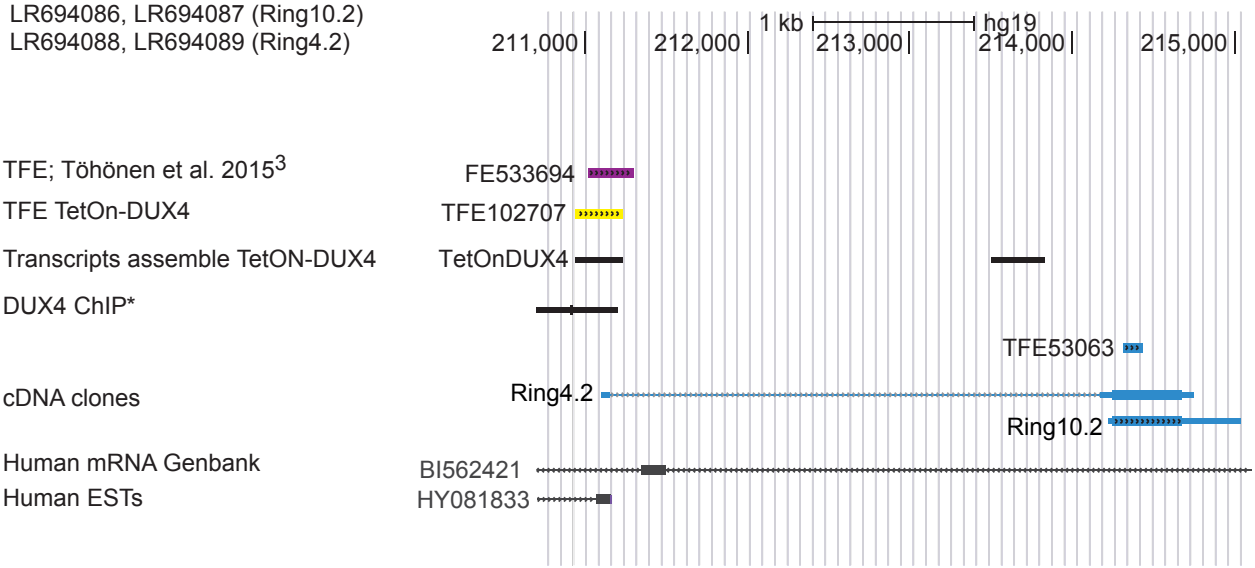

Fig. 7